Pergamon

Int. J. Solids Structures Vol. 34, No. 26, pp. 3415–3432, 1997

0020-7683/97 $17.00 + .00

PII: S0020-7683(96)00225-9

PLASTICITY EFFECTS ON FRACTURE NORMAL TO INTERFACES WITH HOMOGENEOUS AND GRADED COMPOSITIONS

A. S. KIM, S. SURESH
Department of Materials Science and Engineering, Massachusetts Institute of Technology, 77 Massachusetts Avenue, Cambridge, MA 02139-4307, U.S.A.

and

C. F. SHIH
Division of Engineering, Brown University, Providence, RI 02912, U.S.A.

(*Received* 11 *October* 1995; *in revised form* 24 *October* 1996)

Abstract—This paper deals with the problem of a crack in a multi-layered material with a homogeneous or a compositionally graded interface. The effects of plasticity mismatch between the layers (which have no elastic mismatch) on the shielding or amplification of the crack tip driving force are examined by recourse to finite element analyses for the case of a crack perpendicularly approaching the interface between the layers. When the near-tip plastic zone spreads across the interlayer, the crack-tip J integral is smaller than the remotely imposed J integral, if the crack is situated in the plastically weaker material. For this situation, introducing an interlayer between two dissimilar solids provides greater crack-tip shielding than joining the two solids without an interlayer (i.e., with a sharp interface). An interlayer with a homogeneous yield behavior (i.e., where the yield strength of the interlayer is the average of that of the two constituent layers) provides a greater shielding effect than a graded interface within which the yield strength varies linearly from one end of the interlayer to the other. When the crack approaches the interlayer from the plastically stronger material, the crack tip driving force is amplified as the plastic zone spreads across the interlayer. This amplification is the maximum for the interlayer with homogeneous properties, and essentially the same for the situations with a graded interlayer or no interlayer. The dependence of the shielding and amplification effects on the thickness of the interlayer, on the distance from the crack-tip to the interlayer, and on the remote loading are systematically examined. © 1997 Elsevier Science Ltd.

1. INTRODUCTION

A wide variety of technologically significant and fracture-critical composite structures employ metallic materials in conjunction with other metals or ceramics, with the bonding between the dissimilar solids involving interfaces of fixed or spatially varying compositions. Examples include applications in thermal barrier coatings for turbine engines, wear-resistant and contact-fatigue-resistant coatings for a broad range of consumer products, solder joints in microelectronic devices, and weldments and explosion-clad metallic bonds in pressure vessels. In many of these situations, cracks initiate at free surfaces and advance perpendicularly to the interfaces. An understanding of the mechanics and mechanisms of fracture normal to and across the interfaces, as a function of the thickness, mechanical properties, and compositional variations of the interface layer, is essential for failure lifetime analysis and component design.

Fracture mechanics analyses for monotonically loaded cracks intersecting interfaces between two elastic solids perpendicularly have been reported by a number of researchers; see, for example, Zak and Williams (1963), Erdogan and Biricikoglu (1973), Lu and Erdogan (1983), He and Hutchinson (1989), Hutchinson and Suo (1992), Beuth (1992) and Romeo and Ballarini (1996). Small-scale yielding solutions and near-tip fields in which one (or both) of the consitutent materials can deform plastically have been obtained by Ståhle and Shih (1992) and He *et al.* (1996) for stationary crack problems. Plasticity analyses with particular attention to near tip shielding and amplification have been reported

by Sugimura *et al.* (1995a). They showed that cracks which perpendicularly approach interfaces between two metals with the same elastic properties but different plastic properties can experience a reduced or increased effective driving force for fracture as a result of the interaction of the crack-tip plastic zone with the bimaterial interface. Whether the perpendicularly-oriented crack penetrates the interface to continue to advance depends on whether it approaches the interface from the plastically weaker or stronger metal.

Numerical studies in (Sugimura *et al.*, 1995a) reveal that the effective J-integral at the tip of the monotonically loaded stationary crack becomes smaller than the remotely applied J as the plastic zone begins to spread across the interface into the stronger material (when the crack approaches the interface from the weaker material). This "shielding" effect arising from plasticity mismatch between two metals has been demonstrated experimentally by Suresh *et al.* (1992, 1993) who studied fatigue crack growth perpendicular to the interface between a ferritic steel (i.e., plastically weaker solid) and an austenitic steel (the plastically stronger solid) which were joined by explosion cladding. For crack advance under constant applied ΔK, the interaction of the crack-tip plastic zone with the interface resulted in complete crack arrest when the crack approached the interface normally from the ferritic steel. However, the fatigue crack was found to penetrate the interface unimpeded (even showing a slightly accelerated crack growth rate) when the interface was approached by the crack from the austenitic steel. This latter trend of unimpeded advance through the interface is consistent with the predictions of Sugimura *et al.* (1995a) who found that the effective J integral is greater than the remote J (i.e., an amplification in the effective driving force) when the crack approaches the interface from the plastically stronger steel. These experimental and computational studies have clearly established that the plasticity mismatch between interfaces can have a decisive effect on the conditions governing the growth or arrest of cracks. In addition, it is experimentally seen that the trends associated with the growth and arrest of cracks as they approach the interfaces between plastically dissimilar (but elastically similar) materials also carry over to situations when the angle between the crack plane and the plane of the interface is between 0 and 90°, Sugimura *et al.* (1995b).

The aforementioned effects of plasticity on the propensity for fracture across interfaces have been investigated for idealized situations in which the interfaces between the plastically dissimilar solids have been modelled as sharp (i.e., of zero thickness). In reality, however, joining of two metals by such methods as welding, explosion-cladding, or diffusion bonding produces an interface of finite thickness. (In this paper, we refer to such interfaces as interlayers, whose thicknesses are typically smaller than those of the primary constituent layers.) In many applications, such as with thermal/environmental barrier coatings for aircraft engine components or wear-resistant coatings for contact fatigue protection in a number of consumer products, interlayers comprising metal alloys (commonly referred to as "bond coats") are introduced between the metallic substrate and the ceramic protective layer. In the former application the bond coat typically involves a thermally-sprayed NiCrAlY layer, whereas in the latter case a soft layer of Ni-5 wt% Al is deposited on the substrate.

In many layered components, microstructural and compositional gradations invariably occur, either during synthesis and/or in service due to thermal transients, deformation at the interface during joining, or diffusion. For example, heat-affected zones produced in weldments are examples of interface regions wherein the composition and microstructure exhibit large spatial variations. In addition to such "naturally occurring" compositional gradations, it may sometimes be advantageous to create interlayers wherein the composition and properties are intentionally graded in order to achieve a specific function, such as improving interfacial adhesion, lowering thermal residual stresses, minimizing or even fully eliminating stress concentrations at locations where interfaces intersect free surfaces, or enhancing resistance to cracking. Such "functionally graded" interlayers can be produced by means of a number of currently available processing methods which include thermal spray, physical vapor deposition, chemical vapor deposition, powder metallurgy and self-propagating high-temperature combustion synthesis (see, for example, Mortensen and Suresh, 1995). Fracture across such graded interlayers is a topic of considerable interest for a number of potential applications employing functionally graded metallic materials.

The overall motivation of the present work was to develop a comprehensive understanding of the micromechanics of fracture across interfaces of finite thicknesses (interlayers) with fixed or graded compositions/properties between plastically dissimilar solids. This paper seeks to address the following specific issues pertaining to fracture at interlayers.

- To determine the effective J–integral for monotonically loaded, stationary cracks (under small-scale yielding conditions) which perpendicularly approach interlayers between elastically identical but plastically dissimilar solids as a function of
  - the distance of the crack-tip from the interlayer,
  - the direction from which the interlayer is approached (i.e., from the plastically weaker or stronger solid),
  - the thickness of the interlayer,
  - the plastic properties of the interlayer vis-à-vis the plastic properties of the constituent layers,
  - the gradients in plastic properties across the interlayer,
  - the stress state (i.e., plane stress versus plane strain),
- To identify the conditions that determine the continued growth or arrest of cracks as they perpendicularly approach interlayers of fixed or graded compositions,
- To compare the effective driving force for fracture perpendicularly through interlayers with that estimated for a sharp interface (of zero thickness) between the same two constituent layers and
- To develop general guidelines for the effects of plasticity on fracture across interlayers in terms of the role of the geometry and properties of the layers, and the micromechanics of the evolution of crack-tip fields.

2. PLASTICITY-INDUCED CRACK-TIP SHIELDING AND AMPLIFICATION

2.1. *Plasticity-induced load transfer in the trilayer system*

Consider a crack approaching an interlayer joining two substrates possessing identical elastic properties but different plastic properties. We restrict attention to situations involving plastic zones which could be much larger than the distance between the crack tip and the interlayer, but still small compared to the crack length and characteristic dimensions of the crack geometry of interest. Such a problem can be analyzed within a small scale yielding formulation, whereby the actual crack problem is replaced by a semi-infinite crack in an infinite body. Figure 1 shows a semi-infinite crack (perpendicularly) approaching an interlayer joining two semi-infinite substrates. Both Cartesian coordinates x_1, x_2, and polar coordinates r and θ are introduced with their common origin at the tip of the crack. The interlayer has thickness t and its left edge is given by $x_1 = l$. Within a modified boundary layer formulation, the remote field is fully specified by the elastic stress intensity factor K and the T-stress. That is, at large r, the in-plane stress components are of the form

$$\sigma_{ij} = \frac{K}{\sqrt{2\pi r}}\tilde{\sigma}_{ij}(\theta) + T\delta_{1i}\delta_{1j} \tag{1}$$

where $\tilde{\sigma}_{ij}(\theta)$ are known dimensionless angular functions and δ_{ij} is the Kronecker delta.

The elastic properties of substrates 1 and 2 and the interlayer are characterized by Young's Modulus E and Poisson's ratio ν. The plastic properties of the lower strength substrate are characterized by tensile yield strength σ_{Y1} and strain hardening exponent N_1; σ_{Y2} and N_2 characterize the plastic properties of the higher strength material. The plastic properties of the interlayer are spatially nonuniform: the yield strength σ_Y varies linearly from σ_{Y1} to σ_{Y2}. Whereas the strain hardening exponent N can also be chosen to vary gradually, in some prescribed form, from N_1 to N_2, we confine attention to the case where $N_1 = N_2$. This trilayer material system is shown in Fig. 1.

Figure 2 displays the trilayer system in connection with the two crack geometries of interest. In the first, the crack resides in the lower strength material; in the second, it is embedded in the higher strength material. For the moment, the T-stress is taken to vanish;

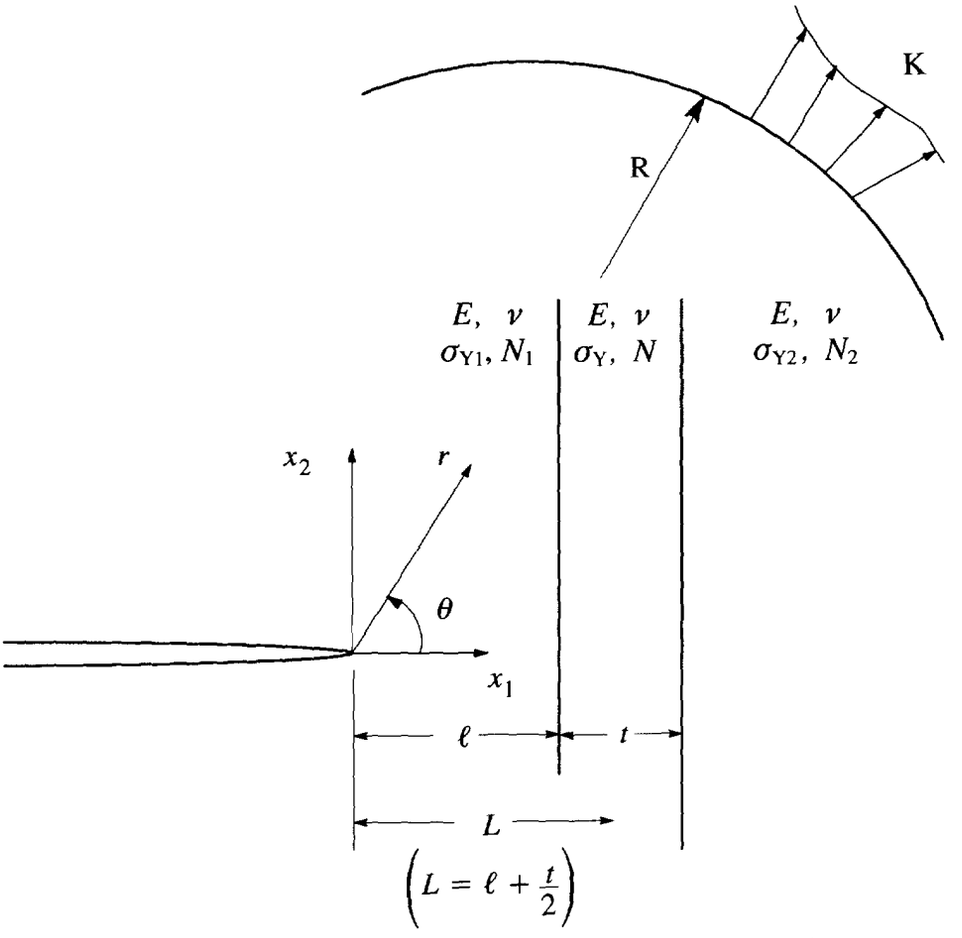

Fig. 1. Crack approaching interlayer of thickness t. Conventions for trilayer material system.

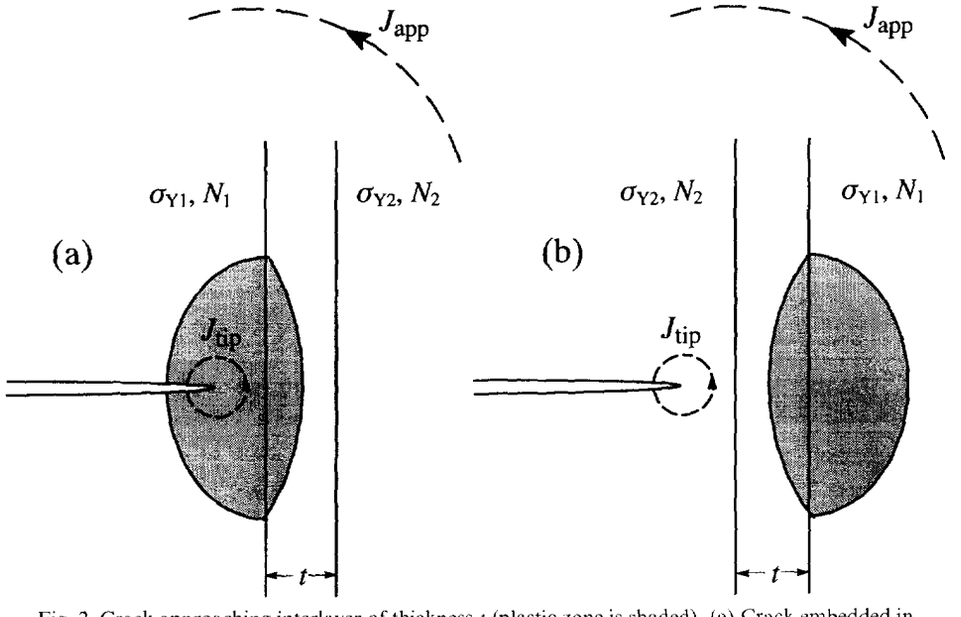

Fig. 2. Crack approaching interlayer of thickness t (plastic zone is shaded). (a) Crack embedded in weak material. $J_{tip} < J_{app}$; crack-tip shielding. (b) Crack embedded in strong material. $J_{tip} > J_{app}$; crack-tip amplification.

its role will be discussed in Section 5. For the purpose of explaining how crack-tip shielding and amplification are induced by plastic flow, it is convenient to consider this limiting case, $\sigma_{Y2} \gg \sigma_{Y1}$; here we specifically examine model systems for which $\sigma_{Y2} = 2\sigma_{Y1}$. Now direct attention to Fig. 2a. It can be easily shown that the stronger material ahead of the plastic zone carries stresses higher than those found at a similar distance ahead of a corresponding crack in a homogeneous material characterized by E, ν, σ_{Y1} and N_1. Transfer of load to the stronger material brings about a stress reduction in the immediate vicinity of the crack, $x_1 < l$. That is, crack tip shielding can arise from plasticity-induced load transfer. Conversely, the shedding of load in the yielded region of the lower material as shown in Fig. 2b elevates the stress in the crack tip region, $x_1 < l$. Therefore, an amplification of the crack tip stress field can be expected for the crack shown in Fig. 2b.

Sugimura *et al.* (1995a) observed that crack-tip shielding and amplification can be quantified by the ratio of two contour evaluations of the J–integral designated by J_{tip} and J_{app}. They noted that the J–integral of Rice (1968) is path-independent in two domains: in the crack tip region $r < l$, and in the remote region. J_{tip} is evaluated by integrating field quantities, obtained from an elastic-plastic finite element analysis, along any contour lying within the crack tip region. This contour is so labelled in Fig. 2 for both crack problems. The applied J can be obtained by integrating field quantities along a remote contour as indicated in Fig. 3. Of course, the applied J is also given by the Rice–Irwin relation,

$$J_{app} = \frac{K^2}{E'} \tag{2}$$

where $E' = E$ for plane stress, and $E' = E/(1-\nu^2)$ for plane strain. Here K is the stress intensity factor, already introduced in (1), which scales with the applied load and a characteristic dimension of the crack geometry. The ratio J_{tip}/J_{app} is the shielding/amplification factor with $J_{tip}/J_{app} < 1$ corresponding to shielding.

2.2. *Evolution of shielding/amplification*

For the bimaterial case considered by Sugimura *et al.* (1995a), where the interlayer thickness was zero, it proved convenient to take the distance from the crack tip to the interface, L, as the normalization factor. For the present trimaterial case, however, we introduce an additional length scale, i.e., the thickness of the interlayer, t. By considering an interlayer of finite thickness to be simply a broadening of the original sharp bimaterial interface, and in order to keep the normalizing lengths consistent with those reported in Sugimura *et al.* (1995a), it proves convenient to introduce a length defined by

$$L = l + \frac{t}{2}, \tag{3}$$

which is the distance between the crack tip and the mid-plane of the interlayer. This enables the systematic incorporation of a homogeneous or a graded interlayer of various thicknesses between the two constituent phases while the location of the interface (i.e., the mid-point of the interlayer) is held fixed. (The results presented in this paper are applicable when t is larger than the size of the fracture process zone.)

A length associated with the spatial variation of the yield strength of the interlayer is $\sigma_{Y1}/(\mathrm{d}\sigma_Y/\mathrm{d}x)$. Therefore, the boundary value problems considered here contain these length scales:

$$L, t, \frac{\sigma_{Y1}}{\mathrm{d}\sigma_Y/\mathrm{d}x_1}, \frac{K^2}{\sigma_{Y1}^2}. \tag{4}$$

We have chosen to normalize K by σ_{Y1}, the yield strength of the weaker material. This normalized load, $(K/\sigma_{Y1})^2$, scales with the plastic zone size in the weaker material. As an

example, Fig. 2 displays the plastic zones in the weaker material indicated by the shaded domains.

Results of plasticity-induced crack-tip shielding and amplification can be conveniently organized about the dimensionless load parameter, $K/(\sigma_{Y1}\sqrt{L})$ (Sugimura *et al.*, 1995a). By dimensional analysis,

$$J_{\text{tip}} = J_{\text{app}} F\left(\frac{K}{\sigma_{Y1}\sqrt{L}}; \frac{t}{L}, \frac{\sigma_{Y1}/t}{\mathrm{d}\sigma_Y/\mathrm{d}x_1}; \frac{\sigma_{Y1}}{\sigma_{Y2}}, \frac{N_1}{N_2}; \frac{\sigma_{Y1}}{E}, N_1, \nu\right) \tag{5}$$

where F is a monotonically increasing, or decreasing, function of the non-dimensional applied load $K/(\sigma_{Y1}\sqrt{L})$. $F < 1$ implies crack-tip shielding while $F > 1$ implies amplification.

In the analysis to follow, only the yield strength is allowed to change, and the same value of N characterizes the strain hardening behavior of the two substrates and the interlayer. For the crack geometry displayed in Fig. 2a, F is unity as long as the plastic zone is confined to substrate 1. Crack-tip shielding takes effect when the plastic zone crosses over into the interlayer and expands into substrate 2. The latter occurs when $K/(\sigma_{Y1}\sqrt{L})$ becomes greater than about 2. Therefore as $K/(\sigma_{Y1}\sqrt{L})$ increases well above 2, F decreases from unity. This reduction from unity represents the amount of shielding. For the crack geometry shown in Fig. 2b, F equals unity in the absence of plastic flow in the interlayer or substrate 2. Crack-tip stress intensification takes effect when a plastic zone develops in substrate 2. This occurs when $K/(\sigma_Y\sqrt{L})$ is greater than about 4. The value of F over and above unity represents the amount of stress intensification.

2.3. *Crack tip fields*

The plastic near-tip field for the crack embedded in an elastic-plastic material (see Fig. 2a) has the form (Hutchinson, 1968; Rice and Rosengren, 1968):

$$\sigma_{ij} = \sigma_Y \left(\frac{J_{\text{tip}}}{\alpha\sigma_Y\varepsilon_Y I_N r}\right)^{N/(1+N)} \tilde{\sigma}_{ij}(\theta; N),$$

$$\varepsilon_{ij} = \alpha\varepsilon_Y \left(\frac{J_{\text{tip}}}{\alpha\sigma_Y\varepsilon_Y I_N r}\right)^{1/(1+N)} \tilde{\varepsilon}_{ij}(\theta; N). \tag{6}$$

Here I_N is an integration constant and $\tilde{\sigma}_{ij}$ and $\tilde{\varepsilon}_{ij}$ are known dimensionless angular functions which depend on N. The material properties in (6) pertain to substrate 1 when the crack is embedded in substrate 1; they pertain to substrate 2 when the crack resides in substrate 2.

In the limiting case, $\sigma_{Y2} \to \infty$, and for the crack embedded in substrate 2, the near tip field can be expressed in the form,

$$\sigma_{ij} = \left(E'\frac{J_{\text{tip}}}{2\pi r}\right)^{1/2} f_{ij}(\theta). \tag{7}$$

Here f_{ij} are well-known dimensionless angular functions obtained from elasticity analysis. The strains are calculated from the usual elastic stress-strain relations.

3. FINITE ELEMENT FORMULATION AND MATERIAL MODEL

In the small scale yielding formulation, incremental tractions consistent with (1) or, equivalently, the incremental displacements according to the K-field solution are applied at the remote boundary as depicted in Fig. 1. In our analyses, the incremental displacements are applied at a distance greater than 10 times the maximum plastic zone size, thereby ensuring that small scale yielding conditions are satisfied. The finite element mesh for the

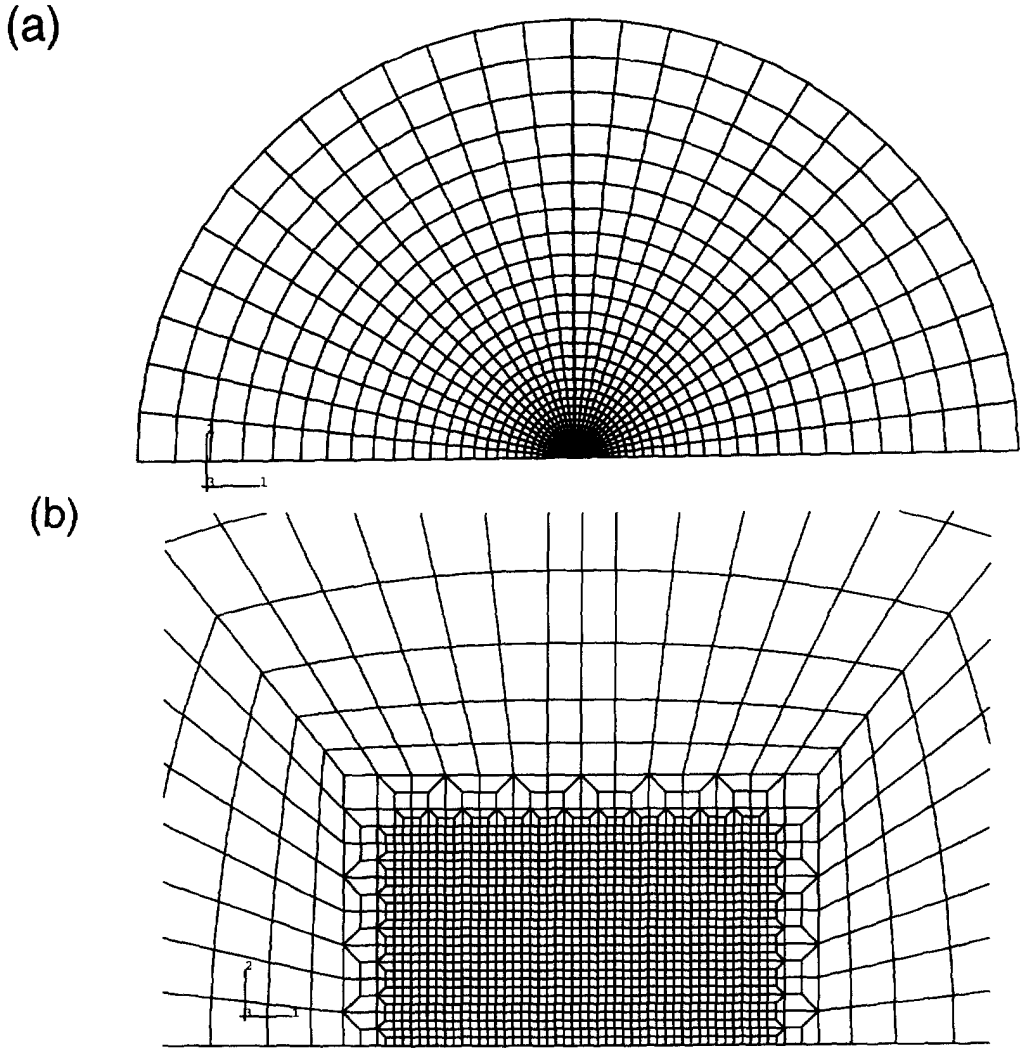

Fig. 3. (a) Finite element mesh for small scale yielding formulation. (b) Refined mesh for near-tip region for crack embedded in weaker substrate.

small scale yielding problem is shown in Fig. 3a; the refined mesh for the near-tip regions is shown in Fig. 3b. This mesh is built up using about 2500, four-noded, bilinear isoparametric elements. Now direct attention to the rectangular region comprising square elements in Fig. 3b. The interlayer has anywhere from 8 to 16 square elements in the thickness direction and 24 square elements in the x_2 direction. The uniform refined mesh region extends for approximately 3 times the interlayer thickness into both the substrates. Beyond the region of uniform mesh, the element sizes are prescribed to increase gradually. Geometries corresponding to $l/t = 0.25$, 0.5, 1.0, 1.5 and 2 are considered in this study. All numerical solutions reported in this paper were obtained with the ABAQUS (1990) finite element program.

The material behavior is taken to be governed by the J_2 flow (rate-independent) theory of plasticity with isotropic hardening. Under uniaxial stressing, the material deforms according to

$$\varepsilon = \frac{\sigma}{E}, \quad \sigma < \sigma_Y,$$

$$= \frac{\sigma_Y}{E}\left(\frac{\sigma}{\sigma_Y}\right)^{1/N}, \quad \sigma \geqslant \sigma_Y. \tag{8}$$

The loads are applied incrementally. As an example, up to 100 displacement increments are taken to reach the maximum K value of interest. The solution to the nonlinear boundary value problem at each increment is obtained by a fully implicit update using the Newton–Raphson method. About six iterations at each increment are sufficient to obtain a convergent solution. Our computational study is performed within a small-displacement-gradient formulation for J_2 flow theory of plasticity.

For a two-dimensional crack problem, the J-integral (Rice, 1968) is defined by

$$J = \int_{\Gamma} \left(W\delta_{1j} - \sigma_{ij} \frac{\partial u_i}{\partial x_1} \right) n_j \mathrm{d}\Gamma. \tag{9}$$

Here, Γ is a contour beginning at the bottom crack face and ending on the top face and n_j is the outward normal to Γ. W is the stress work density computed by following the actual strain history:

$$W = \int_0^{\varepsilon_{pq}} \sigma_{ij} \mathrm{d}\varepsilon_{ij}. \tag{10}$$

The J-integral in ABAQUS is implemented using the domain-integral formulation (Li *et al.*, 1995).

Finite element solutions were also obtained using a J_2 deformation theory of plasticity based on a Ramberg–Osgood description of the material response

$$\varepsilon = \frac{\sigma}{E} + \alpha \frac{\sigma}{E} \left(\frac{\sigma}{\sigma_Y} \right)^{(1-N)/N}. \tag{11}$$

The deformation plasticity computations employ full Newton–Raphson iterations; convergent solutions at selected K levels were obtained within five iterations. The deformation theory solutions for J_{tip} and J_{app} are virtually identical to those obtained under J_2 flow theory; the close agreement strongly suggests that the evolution of the fields near the tip and remote from the tip follows an effectively proportional path. Moreover, the computed J-values for the remote domains are within 2% of the value calculated from (2). These checks attest to the accuracy of the present numerical solutions.

Finite element calculations were performed for both plane stress and plane strain cases. The trends in crack-tip shielding and amplification with $K/(\sigma_{Y1}\sqrt{L})$ and the geometric parameters listed in (5) are similar for plane stress and plane strain. In the interest of space, the discussion will focus on the plane stress results. Plane strain results will be addressed in Section 4.5.

4. NUMERICAL RESULTS

4.1. *Crack approaching the interlayer from the weaker material*

Figure 4 displays the evolution of the shielding factor, $J_{\mathrm{tip}}/J_{\mathrm{app}}$, for the homogeneous interlayer under increasing applied load, $K/(\sigma_{Y1}\sqrt{L})$, with the crack embedded in the weaker material. The five curves correspond to the five geometries, $l/t = 0.25$, 0.5, 1.0, 1.5 and 2. The reader is reminded that l is the distance between the crack tip and the left edge of the interlayer; L is the distance between the crack tip and the mid-plane of the interlayer. It can be seen that shielding takes effect for $K/(\sigma_{Y1}\sqrt{L})$ greater than about 2. For a given load, the greatest shielding occurs for the ratio $l/t = 0.25$ and the least for $l/t = 2.0$, with the most dramatic changes occurring when $l/t < 1.0$, or when the crack tip is less than one interlayer thickness away from the left edge of the interlayer. It may be noted that the case for $l/t \gg 1.0$ approaches the result for the bimaterial problem ($t = 0$).

An analogous case, but with a graded interlayer, is shown in Fig. 5. Again, note that shielding becomes stronger with decreasing l/t and that the most significant increases in

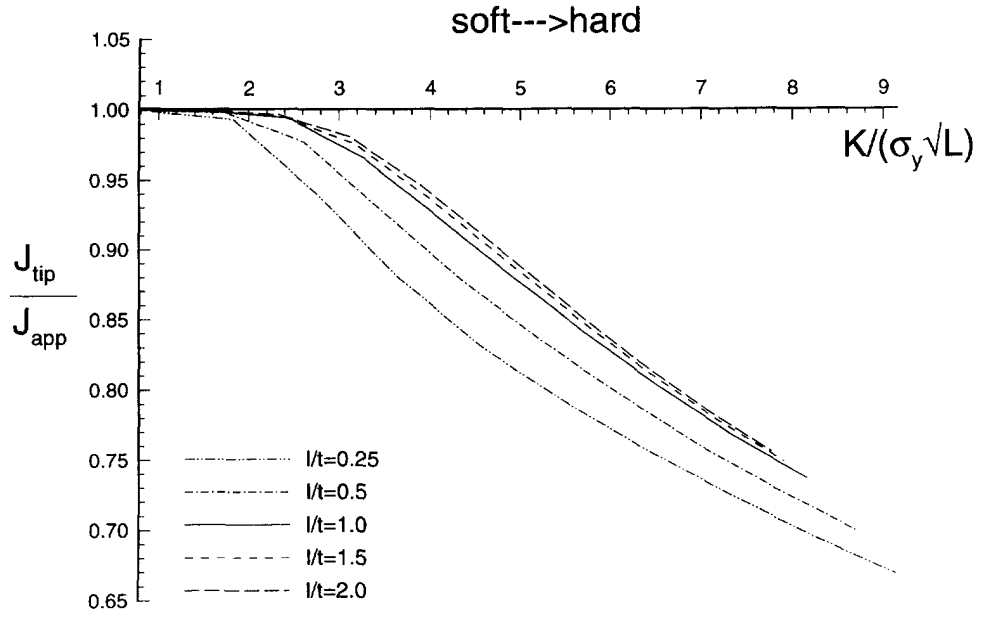

Fig. 4. Evolution of shielding of near-tip fields approaching a homogeneous interlayer under increasing $K/(\sigma_{Y1}\sqrt{L})$. Plane stress results for $l/t = 0.25$, 0.5, 1.0, 1.5 and 2.0.

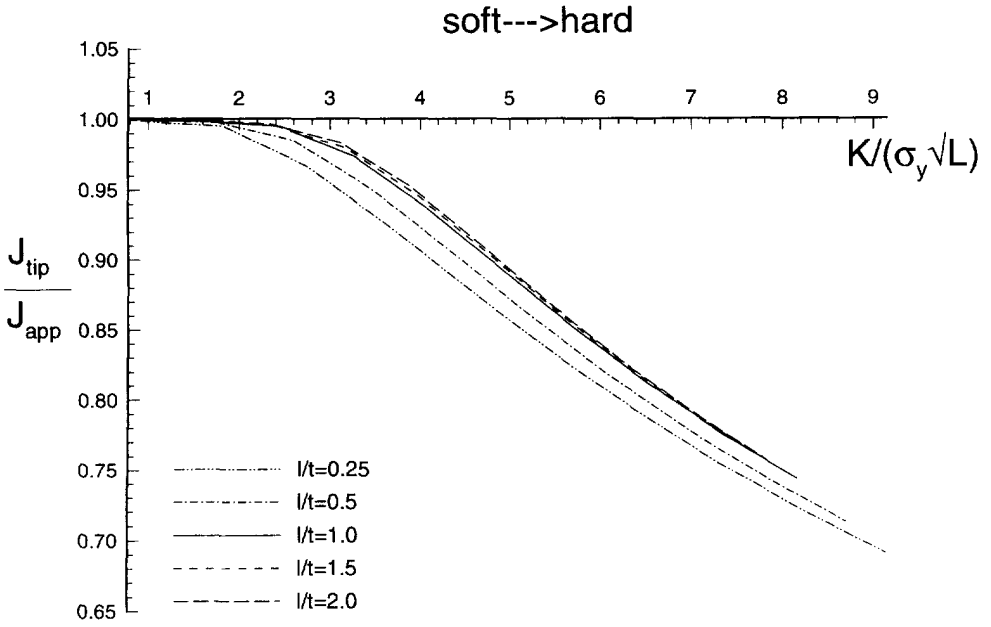

Fig. 5. Evolution of shielding of near-tip fields approaching a graded interlayer under increasing $K/(\sigma_{Y1}\sqrt{L})$. Plane stress results for $l/t = 0.25$, 0.5, 1.0, 1.5 and 2.0.

shielding are observed when $l/t < 1.0$. For the corresponding loads and geometries, the shielding factors for the graded interlayer are generally weaker than those found with the homogeneous interlayer.

4.2. *Crack approaching interface from stronger material*

Figure 6 displays the evolution of the amplification factor, J_{tip}/J_{app}, with a homogeneous interlayer under increasing applied load and the crack embedded in the stronger material. Again, the five curves correspond to the five geometries, $l/t = 0.25$, 0.5, 1.0, 1.5 and 2. Amplification is observed to take effect for $K/(\sigma_{Y1}\sqrt{L})$ greater than about 3 and becomes stronger with decreasing l/t. The greatest effects are observed for the crack tip less than one interlayer thickness away, or when $l/t < 1.0$. In general, the strength of the amplification is

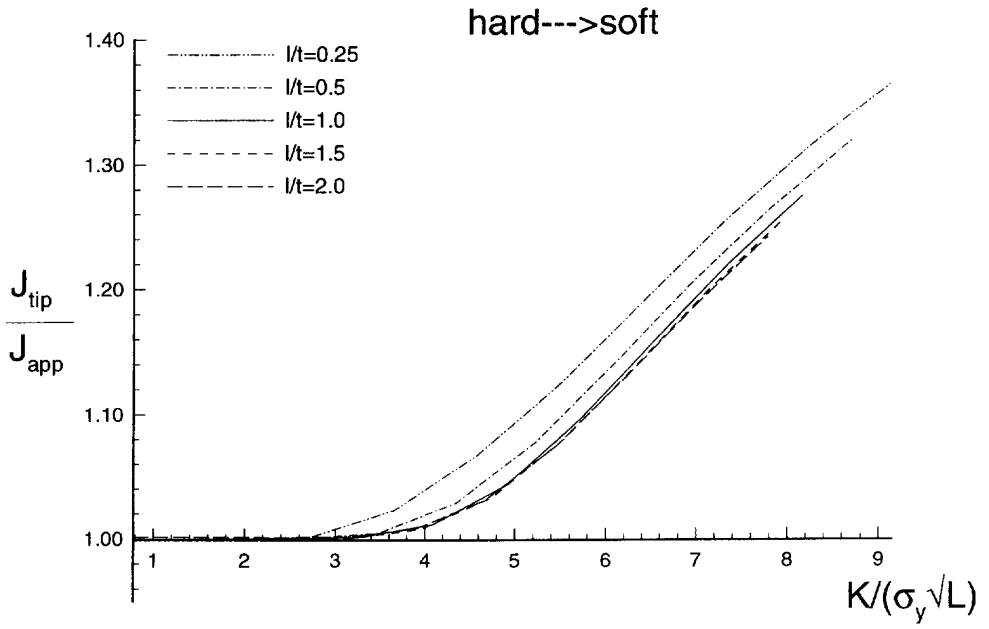

Fig. 6. Evolution of amplification of near-tip fields approaching a homogeneous interlayer under increasing $K/(\sigma_{Y1}\sqrt{L})$. Plane stress results for $l/t = 0.25$, 0.5, 1.0, 1.5 and 2.0.

less severe than the strength of the shielding effects observed with the same geometries and loading conditions.

The case for a crack embedded in the stronger material approaching a graded interlayer is shown in Fig. 7. A slight increase in amplification with decreasing l/t is observed. The differences, however, are less significant than those observed in the other three cases, even when $l/t < 1.0$. As found for the case of shielding when the crack is embedded in the weaker material, the strength of the amplifications is less pronounced for the graded interlayer case than for the homogeneous interlayer.

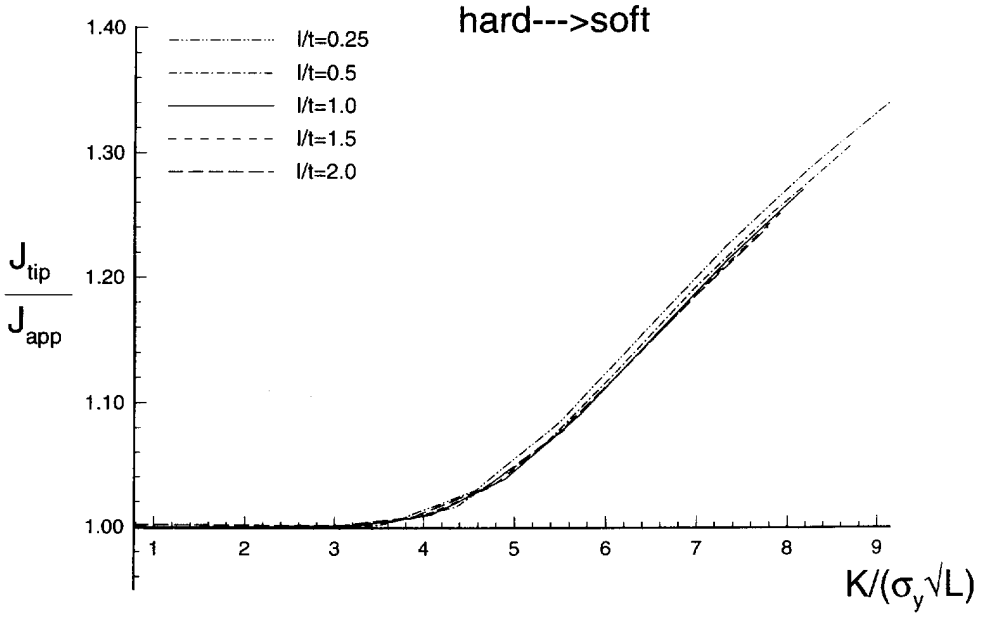

Fig. 7. Evolution of amplification of near-tip fields approaching a graded interlayer under increasing $K/(\sigma_{Y1}\sqrt{L})$. Plane stress results for $l/t = 0.25$, 0.5, 1.0, 1.5 and 2.0.

4.3. *Effects of interactions of crack tip plastic zone with interlayer*

The ratio J_{tip}/J_{app} plotted as a function of $K/(\sigma_Y\sqrt{L})$ is shown in Figs 8(a–d). The four plots represent $l/t = 0.25$, 0.5, 1.0, and 2.0, respectively, for the homogeneous and graded interlayers and their corresponding bimaterials ($t = 0$). Thus, we can directly examine the effects of having a homogeneous or a graded interlayer vis-à-vis a bimaterial with a sharp interface, subjected to the same loading conditions.

In the lower half of each figure, observe that the homogeneous interlayer exhibits the greatest shielding, followed by the graded interlayer and the bimaterial, for each of the geometries and at all loads. The upper half of each figure shows that all three interlayer cases exhibit essentially the same amplification for $l/t > 1$, shown in Fig. 8d; however, the homogeneous interlayer exhibits greater amplification compared to the other two cases, i.e., the graded interlayer and the sharp interface (which are essentially the same) for $l/t \leqslant 1$, as shown in Figs 8a–c.

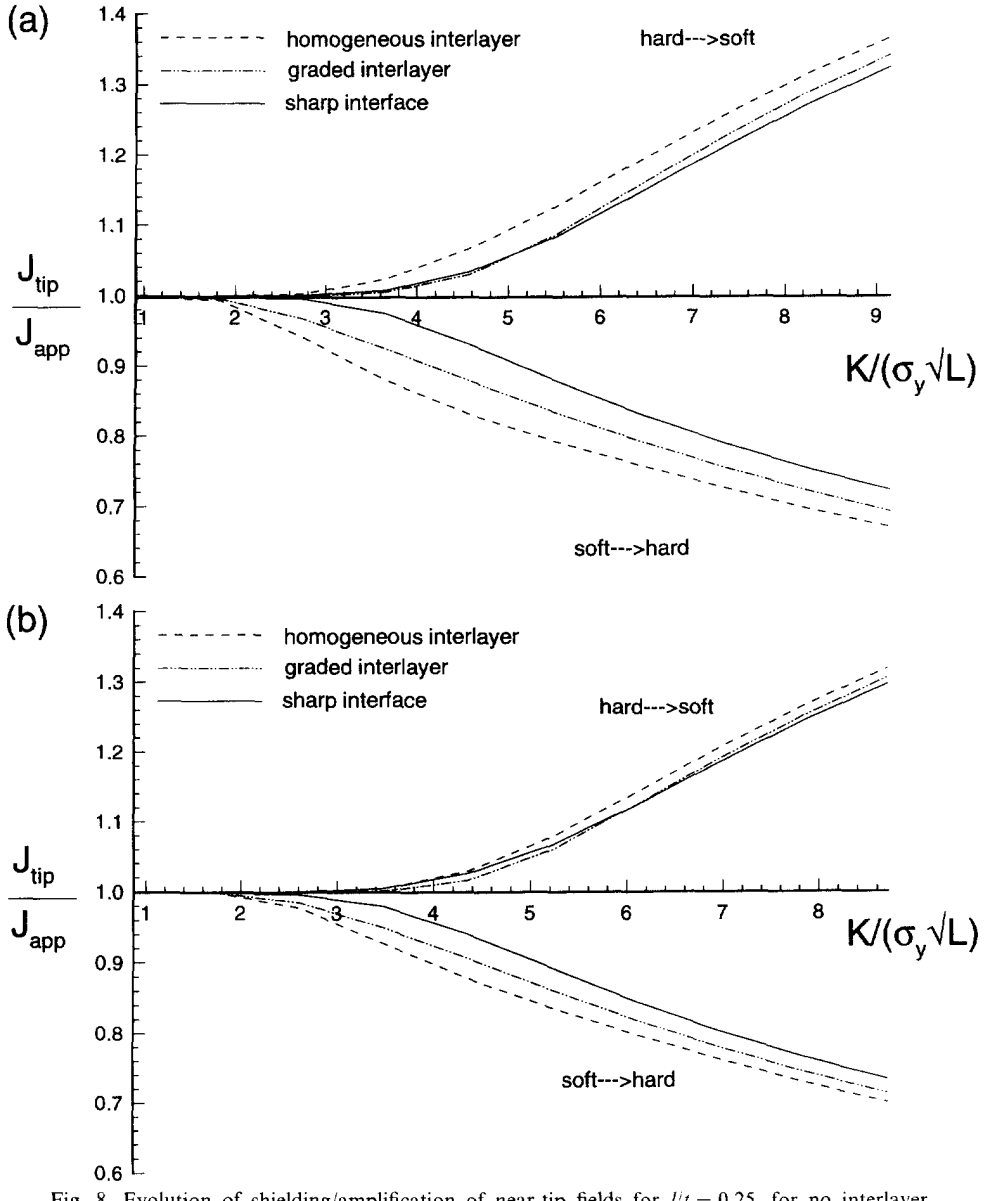

Fig. 8. Evolution of shielding/amplification of near-tip fields for $l/t = 0.25$, for no interlayer, homogeneous interlayer and graded interlayer under increasing $K/(\sigma_{Y1}\sqrt{L})$. (a) $l/t = 0.25$, (b) $l/t = 0.5$, (c) $l/t = 1.0$, (d) $l/t = 2.0$. (*Continued overleaf.*)

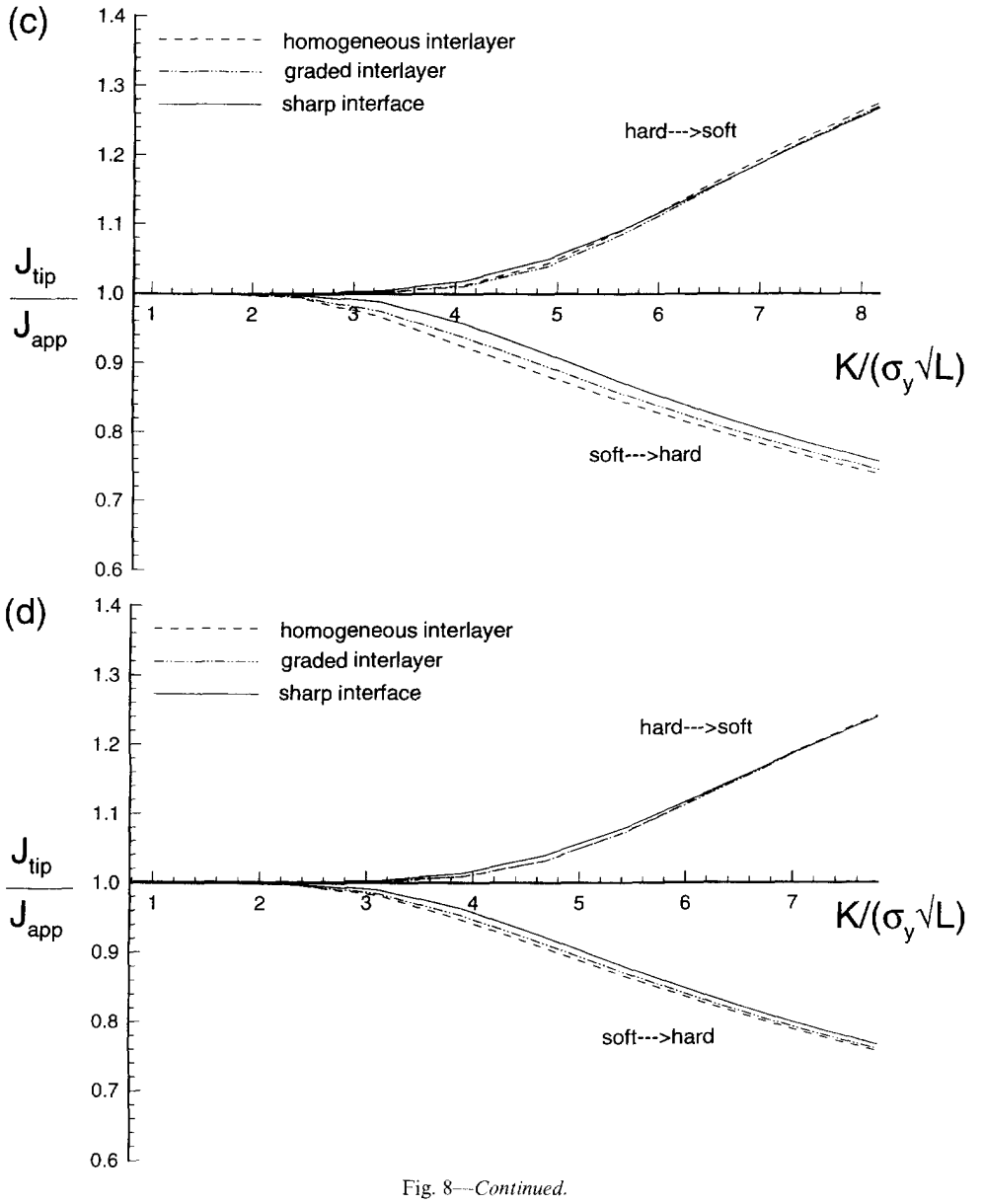

Fig. 8—*Continued.*

4.4. *Crack tip fields*

Figures 9a and 9b show the stress profiles normal to and along the interface, respectively, as a function of distance ahead of the crack tip for a trilayer with the ratio $l/t = 1.0$. Trends for other ratios show similar behavior. Observe that compared to the bimaterial case (no interlayer), the presence of an interlayer reduces the magnitude of the principal stresses ahead of the crack tip. Comparing the two interlayer cases alone, the smooth transition of the σ_{22} stresses obtained due to the presence of the graded interlayer makes it more desirable than a homogeneous interlayer where the stress discontinuities at each of the interfaces could lead to other forms of failure. For the stresses normal to the interfaces, σ_{11}, the graded interlayer is more effective in reducing the magnitude of these stresses compared to the homogeneous interlayer and both interlayer cases induce higher σ_{11} than the bimaterial.

4.5. *Simulations for plane strain*

The foregoing effects of plasticity mismatch on crack tip fields and crack driving force pertained to conditions of plane stress. Figure 10 depicts the evolution of shielding and

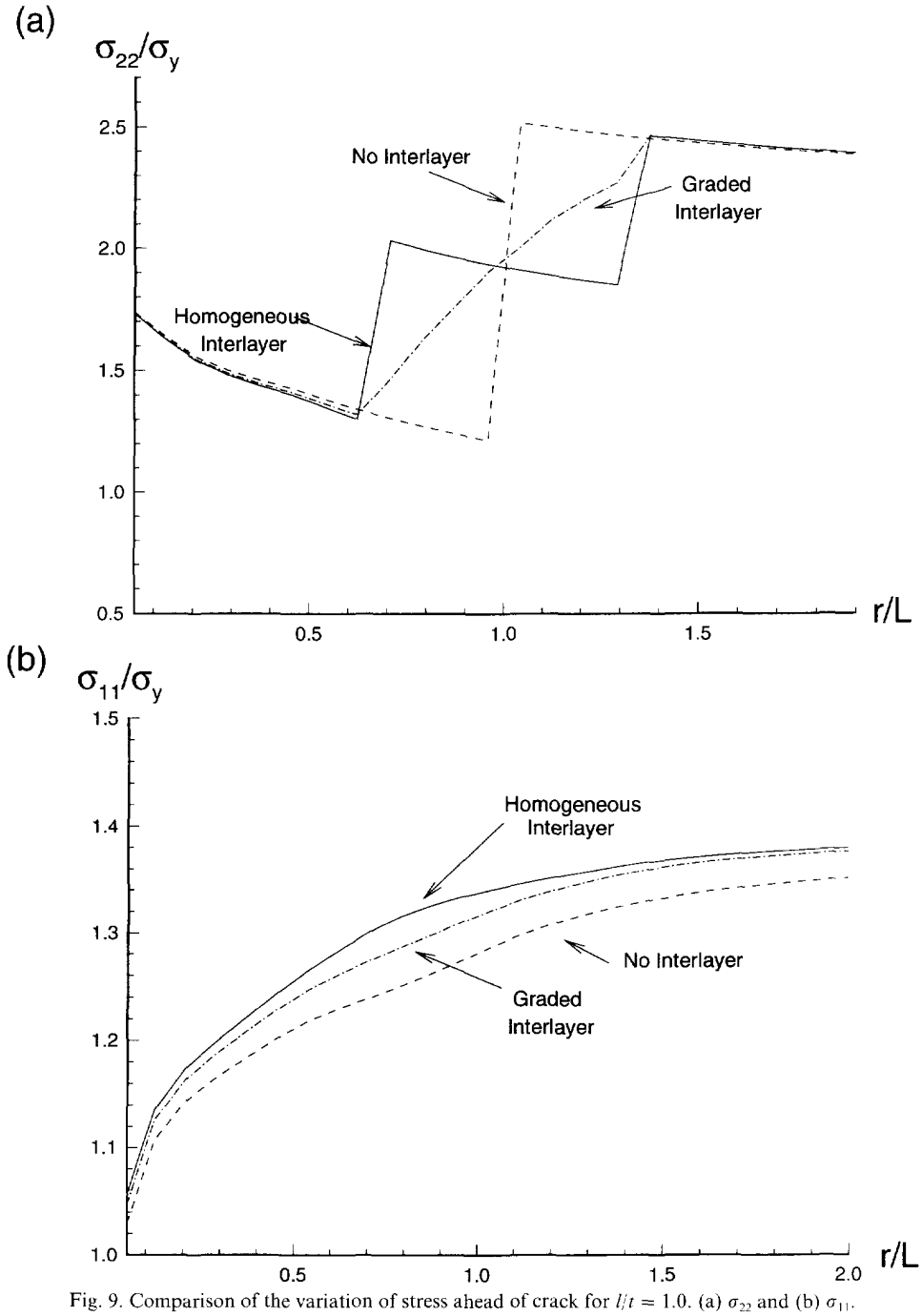

Fig. 9. Comparison of the variation of stress ahead of crack for $l/t = 1.0$. (a) σ_{22} and (b) σ_{11}.

amplification for a homogeneous interlayer under increasing $K/(\sigma_{Y1}\sqrt{L})$ under plane strain conditions (for $l/t = 0.25, 0.5$ and 1.0). Similar results are presented in Fig. 11 for the graded interlayer subject to plane strain. The trends exhibited by both these figures are similar to those seen in Figs 4–7. The only difference seen is that a slightly reduced level of shielding occurs in plane strain than in plane stress, in accordance with expectations.

Figures 12a and 12b show the contour plots of the effective plastic strain ahead of the crack tip for a crack approaching a graded interlayer from the plastically weaker and from the plastically stronger metal, respectively. These plots were obtained for $l/t = 1.0$ and $K/(\sigma_{Y1}\sqrt{L}) = 6.5$. When the plastic zone overlaps the interlayer (with the crack-tip approaching it from the weaker metal), it is seen that plasticity spreads along the boundary with the interlayer within the weaker metal. This causes a much larger, elongated plastic

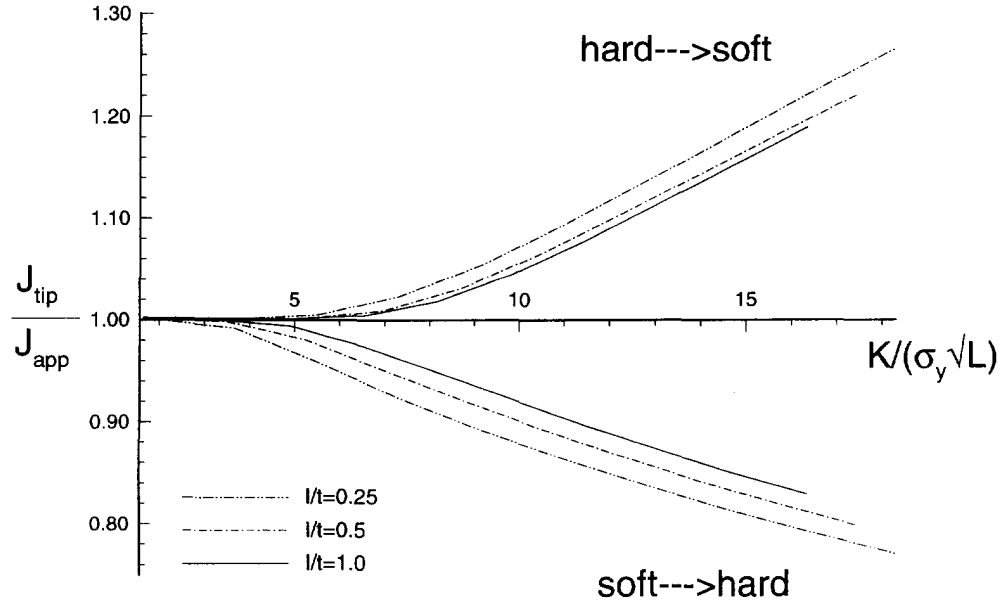

Fig. 10. The evolution of shielding and amplification for a homogeneous interlayer under increasing $K/(\sigma_{Y1}\sqrt{L})$ and for plane strain conditions (for $l/t = 0.25, 0.5$ and 1.0).

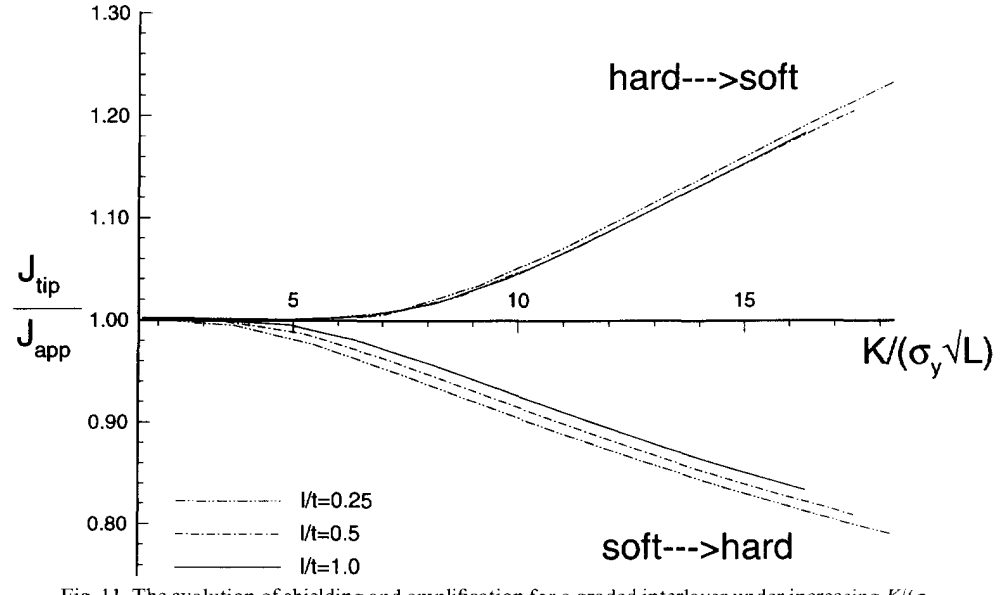

Fig. 11. The evolution of shielding and amplification for a graded interlayer under increasing $K/(\sigma_{Y1}\sqrt{L})$ and for plane strain conditions (for $l/t = 0.25, 0.5$ and 1.0).

zone within the weaker metal than in the stronger metal directly ahead of the crack tip; the interlayer serves to "smoothen" the extent of plastic flow between the two constituent layers. By contrast, a more rounded shape of plastic strain field is observed when the crack tip approaches the interface from the plastically stronger metal (Fig. 12b). A considerably greater spread of the plastic zone occurs in the weaker metal even before the crack-tip begins to penetrate the interlayer. Figures 12a and 12b thus illustrate the significant effect of plastic mismatch in determining the evolution of plastic strains ahead of the crack approaching the interlayer normally. Similar trends (not shown here) were observed for the homogeneous interlayer case; however, the transitions in plastic strains across the interlayer were less gradual compared to those shown in Fig. 12.

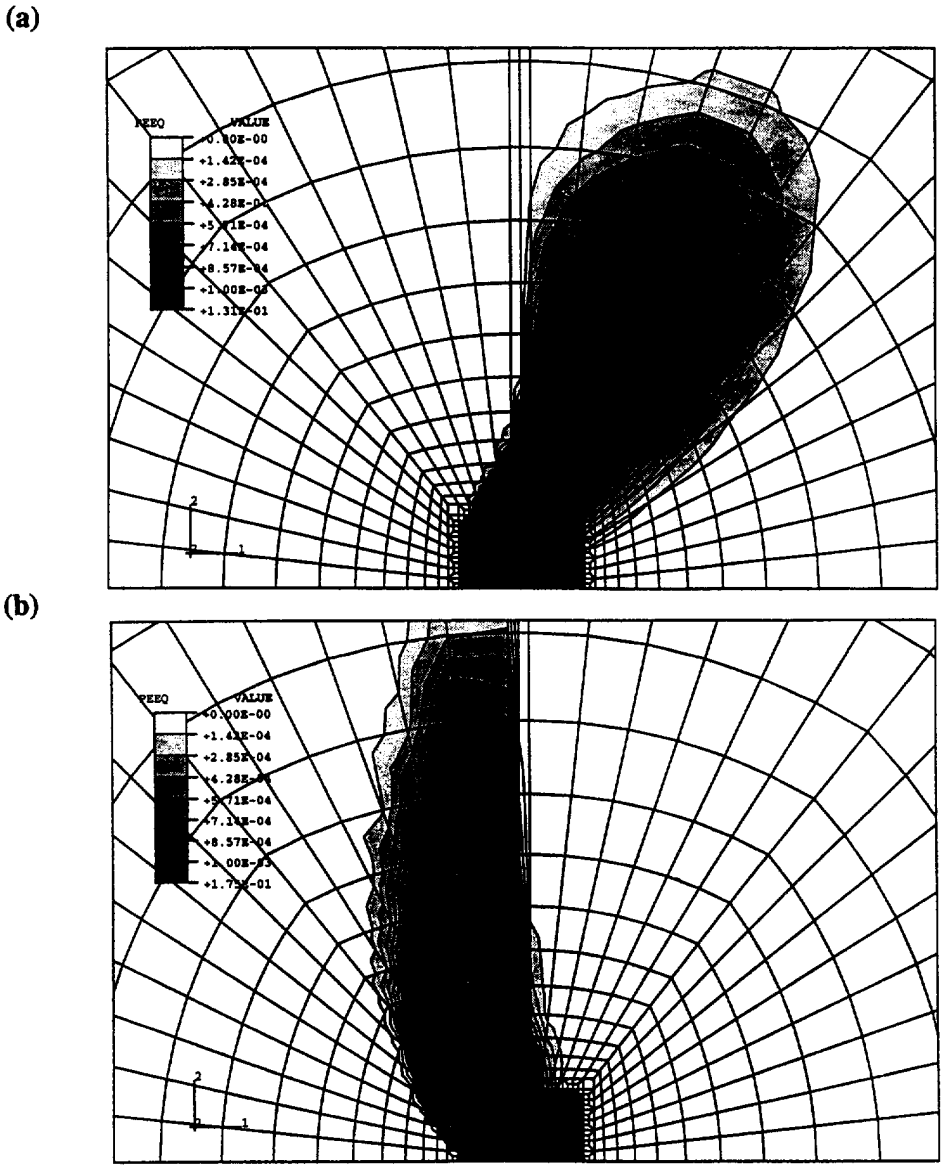

Fig. 12. Contour plots of the effective plastic strain ahead of the crack tip for a crack approaching a graded interlayer from (a) the plastically weaker metal and (b) the plastically stronger metal. These plots were obtained for plane strain and for $l/t = 1.0$ and $K/(\sigma_{Y1}\sqrt{L}) = 6.5$.

5. DISCUSSION

In comparing the bimaterial case with the trilayer case (with a homogeneous interlayer or a graded interlayer), we see that the bimaterial provides both the least shielding (for the crack embedded in the weaker material) and the least amplification (for the crack embedded in the stronger material) of all three cases.

As shown in Section 4.3, a comparison of the two interlayer cases reveals that the graded interlayer provides a beneficial shielding effect compared to the bimaterial, but incurs little detrimental effect with respect to amplification. This is not the case for the homogeneous interlayer which, while providing the most shielding for the crack embedded in the softer material, also causes amplification when the crack is embedded in the harder material. In addition, for a given geometry and loading condition, the maximum spread in the shielding effect (among the different cases studied in Section 4.2) is more pronounced than that in the amplification effect. Furthermore, the magnitude of the change in near-tip driving force as quantified by $|J_{tip}/J_{app} - 1|$, is greater for shielding than for amplification.

Thus, for a given interlayer thickness, the shielding effects will always be more significant than the amplification effects.

Having shown some of the benefits of having a graded interlayer of finite thickness over that of a sharp interface or a homogeneous interlayer, we offer the following line of reasoning to explore the optimum thickness, t, of the graded interlayer to induce the maximum level of shielding. The two extreme cases of interlayer thickness are an interlayer with thickness $t = 0$, which is equivalent to the bimaterial case, and $t = \infty$, which is equivalent to having a homogeneous material. In Fig. 5, it was shown that the shielding effect due to a graded interlayer increases as the ratio l/t decreases, or for the same crack tip position, as t increases. Therefore, it appears desirable to have t as large as possible. When t becomes too large, however, one obtains the limiting case of a homogeneous substrate, and the benefits of having the second material are lost. Therefore, there must be an optimal interlayer thickness.

Sugimura *et al.* (1995a) studied shielding in bimaterial systems ($t = 0$) and showed that shielding becomes significant when the plastic zone begins to interact with the second substrate, or, when $R_p > L$. In the present trilayer problem, shielding takes effect when the plastic zone size R_p is greater than L which is the distance from the crack tip to the center of the interlayer $L = l + t/2$. In addition, although the shielding effects due to the interlayer are always stronger than those for the bimaterial, we can see that the shielding effects of the interlayer are most significant when the ratio $l/t < 1$. Note that for $l/t > 1$, the results approach the bimaterial case which also defeats the purpose of having an interlayer. Thus, t should be made as large as possible while still fulfilling the conditions $R_p > l + t/2$ and $l/t < 1$. Both these conditions are satisfied for an interlayer thickness $t < \frac{2}{3}R_p$.

The analyses conducted in this work have been confined to the case of a stationary crack in a ductile multi-layer system. The present predictions, however, of crack-tip shielding and amplification, arising from plasticity mismatch between two (elastically identical) metals with a finite interlayer thickness, appear to be qualitatively consistent with the experimental results of fatigue crack growth normal to an interlayer (approximately 100 μm in thickness) between a ferritic steel and an austenitic steel (Suresh *et al.*, 1992, 1993, and Sugimura *et al.*, 1995a, b), as described in Section 1. The present analyses thus provide a primary mechanistic justification for the experimental observations of crack retardation (when the crack approaches the interlayer from the weaker ferritic steel) and unimpeded crack advance (when the crack approaches the interlayer from the stronger austenitic steel). A more quantitative comparison of the current predictions with the experimental observations of Suresh *et al.* (1992, 1993) inevitably requires detailed micromechanical analyses of fatigue failure mechanisms (e.g., see Suresh, 1991) and of the role of thermal mismatch stresses in influencing near-tip fields, which is clearly beyond the scope of this work.

The experiments of Suresh *et al.* (1992, 1993) also reveal that when fatigue crack arrest occurs in the weaker steel, the plane of the crack deviates from the nominal mode I growth plane (which is normal to the interlayer). We provide the following line of reasoning, predicated upon the role of T-stress in influencing the crack path, in an attempt to shed some light on this crack deflection mechanism.

T-stress effects on crack tip shielding and amplification have been discussed by Sugimura *et al.* (1995a); the reader is referred to Section 5 of that paper for a more complete discussion. Sugimura *et al.* found that both crack tip shielding and amplification are intensified by a negative T-stress. In contrast, a positive T-stress exerts minimal effect on shielding and amplification, unless the T-stress in question approaches the yield strength. These effects can be explained in terms of the highly nonlinear dependence of the plastic zone size on T-stress which has the form:

$$R_p = \Lambda(T/\sigma_Y)\left(\frac{K}{\sigma_Y}\right)^2. \tag{12}$$

Here σ_Y is the yield stress of the lowest strength material and Λ depends additionally on the ratio of the yield strengths of the two substrates (Λ is weakly dependent on the material

and geometric parameters of the layered system listed as the arguments in eqn (5)). It has been established in several studies (e.g., Shih *et al.*, 1993) that Λ increases rapidly under a negative T-stress and

$$\frac{\Lambda(T/\sigma_Y \leqslant -0.5)}{\Lambda(T/\sigma_Y = 0)} \gg 1. \tag{13}$$

The strong dependence of Λ on T-stress can be seen in Fig. 4 of Shih *et al.*

In addition to what has been noted above, Cotterell and Rice (1980) have shown that crack propagation is directionally stable if $T < 0$ and unstable if $T > 0$. It is known that T-stress is negative for compact tension specimens with crack length to width ratios, a/W, less than 0.3; T-stress is positive for a/W greater than 0.3. Therefore it is possible for a crack to advance under a negative T-stress initially. After a sufficient amount of growth, the crack can be subject to a positive T-stress. A positive T-stress can also arise from plastic deformation near an interface between two substrates of strongly differing yield strengths. This deformation-induced T-stress can become significant when the crack residing in the softer layer approaches the interlayer or interface (geometry depicted in Fig. 2a). Both deformation- and crack growth-induced T-stresses favor crack deflection which is also beneficial. Interestingly enough, evidence for crack deflection has been reported in the experiments where the fatigue crack approaches the interlayer from the plastically weaker ferritic steel (Suresh *et al.*, 1992, 1993).

The process of joining two different materials usually results in a diffusion or reaction interlayer of finite thickness. The problem under study can be viewed in the following way. A material layer with finite dimensions is joined to a substrate. That is, in relation to Fig. 1, the length L can be regarded as unchanging. Given that L is the characteristic dimension of the layered geometry, we address the effects induced by the existence (formation) of an interlayer of thickness t as depicted in Fig. 1. The length ℓ is defined by $L-(t/2)$ and is superfluous when $t = 0$.

6. CONCLUSIONS

In this work, we have reported the results of a finite element study which has quantified the role of plasticity mismatch on the driving force and near-tip fields for stationary cracks which approach interfaces perpendicularly in layered materials (with no mismatch in elastic properties). It is shown that, when the near-tip plastic zone overlaps with the interlayer, the crack-tip J integral, J_{tip}, becomes smaller than the remotely imposed J integral, J_{app}, if the crack is situated in the plastically weaker material. An interlayer with a homogeneous yield behavior (i.e., where the yield strength of the interlayer is the average of that of the two constituent layers) provides a greater shielding effect than a graded interface within which the yield strength varies linearly from one end of the interlayer to the other. When the crack approaches the interlayer from the plastically stronger material, an amplification in the crack tip driving force is observed (i.e., $J_{tip}/J_{app} > 1$). This amplification is the maximum for the interlayer with homogeneous properties, and essentially the same for the situations with a graded interlayer or no interlayer. The dependence of the shielding and amplification effects on the thickness of the interlayer, on the distance from the crack-tip to the interlayer, and on the remote loading are systematically examined. Geometrical features of the interlayer which provide the most beneficial shielding effect are identified. The predictions of the finite element analyses are found to be in qualitative agreement with the experimental observations of Suresh *et al.* (1992, 1993) for fatigue crack growth normal to steel-steel bimaterial interfaces.

Acknowledgments—This work was carried out at the Laboratory for Experimental and Computational Micromechanics at MIT and supported by the U.S. Department of Energy under Grant DE-FG02-93ER45506 to MIT. ASK and CFS acknowledge partial support from Grant N61533-93-K-0030 from the U.S. Nuclear Regulatory Commission. Helpful discussions with M. Finot are also acknowledged.

REFERENCES

ABAQUS User's Manual, Version 4.8, (1990) Hibbitt, Karlsson and Sorensen, Inc., Providence, RI.

Beuth, J. L., Jr. (1992) Cracking of thin bonded films in residual tension. *International Journal of Solids and Structures* **29,** 1657–1069.

Cotterell, B. and Rice, J. R. (1980) Slightly curved or kinked cracks. *International Journal of Fracture* **16,** 155–169.

Erdogan, F. and Biricikoglu, V. (1973) Two bonded half planes with a crack going through the interface. *International Journal of Engineering Science* **11,** 745–766.

He, M. Y., Ståhle, P., Shih, C. F., Zhang, N. T. and McMeeking, R. M. (1996) Crack terminating perpendicularly at interface between dissimilar materials—small-scale yielding analysis (submitted).

He, M. Y. and Hutchinson, J. W. (1989) Crack deflection at an interface between dissimilar elastic materials. *International Journal of Solids and Structures* **25,** 1053–1069.

Hutchinson, J. W. (1968) Singular behaviour at the end of a tensile crack in a hardening material. *Journal of Mechanics and Physics of Solids* **16,** 13–31.

Hutchinson, J. W. and Suo, Z. (1992) Mixed mode cracking in layered materials. *Advances in Applied Mechanics* **29,** 63–191.

Li, F. Z., Shih, C. F. and Needleman, A. (1985) A comparison of methods for calculating energy release rates. *Engineering Fracture Mechanics* **21,** 405–421.

Lu, M. C. and Erdogan, F. (1983) Stress intensity factors in two bonded elastic layers containing cracks perpendicular to and on the interface. *Engineering Fracture Mechanics* **18,** 491–528.

Mortensen, A. and Suresh, S. (1995) Functionally graded metals and metal-ceramic composites Part I. Processing. *International Material Review* **40,** 239–265.

Rice, J. R. (1968) A path independent integral and the approximate analysis of strain concentration by notches and cracks. *Journal of Applied Mechanics* **35,** 379–386.

Rice, J. R. and Rosengren, G. F. (1968) Plane strain deformation near a crack tip in a power-law hardening material. *Journal of Mechanics and Physics Solids* **16,** 1–12.

Romeo, A. and Ballarini, R. (1996) A crack very close to a bimaterial interface. *Journal of Applied Mechanics* (in press).

Shih, C. F., O'Dowd, N. P. and Kirk, M. T. (1993) A framework for quantifying crack tip constraint. In *Constraint Effects in Fracture*, ASTM STP 1171, eds E. M. Hackett, *et al.* American Society for Testing and Materials, Philadelphia, pp. 2–20.

Ståhle, P. and Shih, C. F. (1992) Cracking in thin films and substrates. *Proceedings of Material Research Society Symposium* **239,** 567–572.

Sugimura, Y., Lim, P. G., Shih, C. F. and Suresh, S. (1995a) Fracture normal to a bimaterial interface : effects of plasticity on crack-tip shielding and amplification. *Acta Metallica Materiala* **43,** 1157–1169.

Sugimura, Y., Grondin, L. and Suresh, S. (1995b) Fatigue crack growth at arbitrary angles to bimaterial interfaces. *Scripta Metallica Materiala* **33,** 2007–2012.

Suresh, S. (1991) *Fatigue of Materials*. Cambridge University Press, Cambridge, U.K.

Suresh, S., Sugimura, Y. and Tschegg, E. K. (1992) The growth of a fatigue crack approaching a perpendicularly-oriented bimaterial interface. *Scripta Metallica Materiala* **27,** 1189–1194.

Suresh, S., Sugimura, Y. and Ogawa, T. (1993) Fatigue cracking in materials with brittle surface-coatings. *Scripta Metallica Materiala* **29,** 237–242.

Zak, A. R. and Williams, M. L. (1963) Crack point singularities at a bi-material interface. *Journal of Applied Mechanics* **30,** 142–143.